arXiv:hep-ph/0406123v1 10 Jun 2004

LC–PHSM–2003–071
August 2003

Study of Sleptons at a Linear Collider – Supersymmetry Scenario SPS 1a[*]

Hans-Ulrich Martyn[†]
I. Physikalisches Institut, RWTH Aachen, Germany

The properties of the light charged sleptons in $\tilde{e}_R\tilde{e}_R$, $\tilde{\mu}_R\tilde{\mu}_R$ and $\tilde{\tau}_1\tilde{\tau}_1$ production are studied within the mSUGRA scenario SPS 1a. Various method are presented to determine very precisely masses, angular distributions, spin and couplings as well as the $\tilde{\tau}_1$ polarisation and mixing parameter in the $\tilde{\tau}$ sector. The analysis is based on a complete simulation of signal and background reactions assuming experimental conditions of the TESLA e^+e^- Linear Collider.

1 Introduction

This note describes, for a particular bench mark model, how masses and couplings of scalar leptons can be accurately measured at a future e^+e^- linear collider TESLA [1]. Beam conditions are chosen such as to stay below production thresholds of the heavier sleptons, the assumed luminosity corresponds to about one year of running at design parameters. Details of the experimental simulation, analysis and background information on kinematics and theory are given in sketchy form.

Particle spectrum mSUGRA SPS 1a scenario [2] (parameters $m_0 = 100$ GeV, $m_{1/2} = 250$ GeV, $A_0 = -100$ GeV, $\tan\beta = 10$, sign $\mu +$) shown in fig. 1. Cascade decays of $\tilde{\chi}^0_2$, $\tilde{\chi}^\pm_1$ lead to abundant τ final states.

Event generation PYTHIA 6.2 [3] including beam polarisations $\mathcal{P}_{e^\pm}$, QED radiation, beamstrahlung à la CIRCE [4], τ decays and τ polarisation treated by TAUOLA [5]

---

[*] Contribution to the Extended ECFA/DESY Study on Physics and Detectors for a Linear Electron-Positron Collider (2001 – 2003)

[†] email: martyn@mail.desy.de

Operating conditions $\sqrt{s} = 400$ GeV, beam polarisations $\mathcal{P}_{e^-} = +0.80$, $\mathcal{P}_{e^+} = -0.60$, integrated luminosity $\mathcal{L} = 200\ \mathrm{fb}^{-1}$
⇒ efficient suppression of SUSY ($\tilde{\nu}_l,\ \tilde{\chi}^0_2,\ \tilde{\chi}^\pm_1$) and SM background

Detector à la TDR [1] Simulation based on SIMDET 4.02 [6], acceptance $\theta > 125$ mrad, $e,\ \gamma$ veto $\theta > 4.6$ mrad

Slepton production

$$
\begin{aligned}
e^+_L e^-_R &\to \tilde{\mu}_R \tilde{\mu}_R \qquad (120\,\mathrm{fb}) && (1)\\
e^+_L e^-_R &\to \tilde{e}_R \tilde{e}_R \qquad (550\,\mathrm{fb}) && (2)\\
e^+_L e^-_R &\to \tilde{\tau}_1 \tilde{\tau}_1 \qquad (140\,\mathrm{fb}) && (3)
\end{aligned}
$$

Background production SUSY bkg $e^+_L e^-_R \to \tilde{e}_R \tilde{e}_L\ (75\,\mathrm{fb}),\ \tilde{\chi}^0_2 \tilde{\chi}^0_1\ (20\,\mathrm{fb}),\ \tilde{\chi}^+_1 \tilde{\chi}^+_1\ (5\,\mathrm{fb})$
SM bkg $e^+_L e^-_R \to W^+ W^-\ (1000\,\mathrm{fb})\ [B_{W\to\ell\nu} = 0.107]$, $e^+ e^- \to \ell^+ \ell^- (\gamma)$ negligible
$\gamma\gamma$ bkg negligible $\sigma(e^+e^- \to e^+e^-\tau^+\tau^-) = 4.5 \cdot 10^5$ fb, acceptance $<$ few10^{-6}

Slepton decays

$$
\tilde{\ell}^- \to \ell^- \ \tilde{\chi}^0_1 \tag{4}
$$

Flat lepton energy spectrum with endpoints $E_{+/-}$ related to slepton and neutralino masses

$$
\begin{aligned}
E_{+/-} &= \frac{\sqrt{s}}{4}\left(1 - \frac{m^2_{\tilde{\chi}}}{m^2_{\tilde{\ell}}}\right)(1 \pm \beta) && (5)\\
m_{\tilde{l}} &= \frac{\sqrt{s}}{E_- + E_+}\sqrt{E_- E_+} && (6)\\
m_{\tilde{\chi}} &= m_{\tilde{l}}\sqrt{1 - \frac{E_- + E_+}{\sqrt{s}/2}} && (7)
\end{aligned}
$$

$\ell^+\ell^-$ momentum correlations [7]
$m_{\tilde{\chi}^0}$ known: energy-momentum conservation constrains construction of kinematically allowed minimum mass $m_{\min}(\tilde{\ell})$ sharp peak around true mass $m_{\tilde{\ell}}$

$m_{\tilde{\chi}^0}$ and $m_{\tilde{\ell}}$ known: reconstruct $\tilde{\ell}$ direction θ
two-fold ambiguity, false solution flat in $\cos\theta$

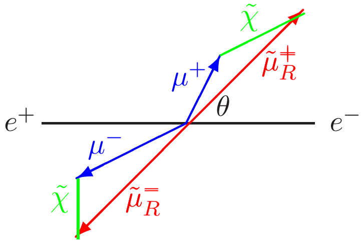

2 Properties of smuons

Selection criteria $e^+_L e^-_R \to \tilde{\mu}_R \tilde{\mu}_R$ at $\sqrt{s} = 400$ GeV

```
nr  cut                                 min       max      eff
-------------------------------------------------------------
 0. n_ch, n_gamma in accept.              2         0     0.815
    n_charge in acceptance                2         2     0.989
    n_gamma  in acceptance              5.0         0     0.851
    n_veto   in acceptance              5.0         0     0.960
 1. Q*cos_theta_l                    -0.900     0.750     0.693
 2. delta phi_(l+,l-) (deg)                     160.0     0.555
 4. p_T event (GeV)                    10.0               0.553
 5. p_miss cos_theta_(l+l-)                     0.900     0.537
 7. lepton energy (GeV)                 2.5     150.0     0.537
10. m_recoil + 0.4*m_ll (GeV)         240.0               0.537

 efficiency     0.5365

 lepton energy  E_min 16.52       E_max 93.30
```

Mass determination Spectra of the muon energy E_μ and minimum mass $m_{\rm min}(\tilde{\mu}_R)$ are shown in fig. 2. The endpoint energies, $E_- = 16.570 \pm 0.040$ GeV and $E_+ = 93.30 \pm 0.22$ GeV, give strongly correlated $\tilde{\mu}_R$ and $\tilde{\chi}^0_1$ masses. The reconstructed masses from both methods agree well with the input values.

method	$m_{\tilde{\mu}_R}$ [GeV]	$m_{\tilde{\chi}^0_1}$ [GeV]
E_μ **spectrum**	$\mathbf{143.15 \pm 0.17}$	$\mathbf{96.10 \pm 0.21}$
$m_{\rm min}(\tilde{\mu}_R)$ **spectrum**	$\mathbf{142.98 \pm 0.03}$	**fixed**
SPS 1a input	**143.0**	**96.0**

Spin $J = 0$ of $\tilde{\mu}_R$ The polar angle distribution of $\tilde{\mu}_R \tilde{\mu}_R$ production is presented in fig. 3. After background subtraction on finds the typical cross section dependence

$$\frac{\mathrm{d}\sigma}{\mathrm{d}\cos\theta} \quad \propto \quad \sin^2\theta$$

as expected for a scalar particle.

3 Properties of selectrons

Selection criteria $e^+_L e^-_R \to \tilde{e}_R \tilde{e}_R$ at $\sqrt{s} = 400$ GeV

```
nr  cut                                 min       max      eff
-------------------------------------------------------------
 0. n_ch, n_gamma in accept.              2         0     0.742
    n_charge in acceptance                2         2     0.984
    n_gamma  in acceptance              5.0         0     0.780
    n_veto   in acceptance              5.0         0     0.960
 1. Q*cos_theta_l                 -0.900     0.750     0.586
 2. delta phi_(l+,l-) (deg)                  160.0     0.484
 4. p_T event (GeV)                 10.0               0.484
 5. p_miss cos_theta_(l+l-)                  0.900     0.468
 7. lepton energy (GeV)              2.5     150.0     0.468
10. m_recoil + 0.4*m_ll (GeV)      240.0               0.468

 efficiency     0.4675

 lepton energy  E_min 16.52       E_max 93.30
```

Mass determination Spectra of the electron energy E_e and minimum mass $m_{\min}(\tilde{e}_R)$ are shown in fig. 4. The endpoint energies, $E_- = 16.528 \pm 0.020$ GeV and $E_+ = 93.34 \pm 0.11$ GeV, give strongly correlated $\tilde{e}_R$ and $\tilde{\chi}^0_1$ masses. The reconstructed masses from both methods are in agreement with the input values.

method	$m_{\tilde{e}_R}$ **[GeV]**	$m_{\tilde{\chi}^0_1}$ **[GeV]**
E_e **spectrum**	$\mathbf{142.99 \pm 0.08}$	$\mathbf{96.05 \pm 0.10}$
$m_{\min}(\tilde{e}_R)$ **spectrum**	$\mathbf{142.97 \pm 0.02}$	**fixed**
SPS 1a input	**143.0**	**96.0**

Angular distribution of $\tilde{e}_R$ The polar angle distribution of $\tilde{e}_R\tilde{e}_R$ production is presented in fig. 5. After background subtraction on finds the typical behaviour of t-channel neutralino exchange, given by the approximate matrix element

$$\mathcal{M} \quad \sim \quad \beta \sin\theta \left[1 - \frac{4\, Y^2_{\tilde{B}}}{1 - 2\,\beta\, \cos\theta + \beta^2 + 4\, M_1^2/s} \right] \; .$$

The differential cross section can be used to determine the Yukawa coupling $Y_{\tilde{B}} = \hat{g}'_{\tilde{B}\tilde{e}e}/g'_{\gamma ee}$ and the gaugino mass parameter M_1 at the percent level.

Chiral quantum numbers A unique determination of the selectron L/R quantum numbers is offered by the reaction $e^+e^- \to \tilde{e}_R\tilde{e}_L$, which proceed via pure t-channel $\tilde{\chi}^0$ exchange. The ‘chiral flow’ at the $e\tilde{\chi}^0\tilde{e}$ vertex associates the incoming electron/positron with its superpartner: $e^-_L \to \tilde{e}^-_L$, $e^-_R \to \tilde{e}^-_R$ and $e^+_L \to \tilde{e}^+_R$, $e^+_R \to \tilde{e}^+_L$. Measuring the energy spectra of the decay e^- and e^+ separately allows for a clear distinction between $\tilde{e}_R$ and $\tilde{e}_L$. Moreover, by choosing appropriate beam polarisations, *e.g.* ‘odd’ combinations $e^+_R e^-_R \to \tilde{e}^+_L\tilde{e}^-_R$ or $e^+_L e^-_L \to \tilde{e}^+_R\tilde{e}^-_L$, one suppresses the s-channel γ, Z amplitudes of $\tilde{e}_R\tilde{e}_R$ and other background and enhances the $\tilde{e}_R\tilde{e}_L$ production considerably, as illustrated in fig. 6 and fig. 7. Contributions from $\tilde{e}_R\tilde{e}_R$ are identical in both $e^\pm$ spectra and can be readily subtracted since $m_{\tilde{e}_R}$ is known. A measurement of the $\tilde{e}_L$ mass of $m_{\tilde{e}_L} = 202.1 \pm 0.5$ GeV appears feasible. Similar studies are reported in [8].

4 Properties of staus

Parameters $L-R$ mixing in third generation, access to $\tan\beta$ and A_τ [9, 10]

$$\begin{pmatrix} \tilde{\tau}_1 \\ \tilde{\tau}_2 \end{pmatrix} = \begin{pmatrix} \cos\theta_{\tilde{\tau}} & \sin\theta_{\tilde{\tau}} \\ -\sin\theta_{\tilde{\tau}} & \cos\theta_{\tilde{\tau}} \end{pmatrix} \begin{pmatrix} \tilde{\tau}_L \\ \tilde{\tau}_R \end{pmatrix} \tag{8}$$

$$\tan 2\,\theta_{\tilde{\tau}} = \frac{-2\,m_\tau\,(A_\tau - \mu\tan\beta)}{m^2_{\tilde{\tau}_R} - m^2_{\tilde{\tau}_L}} \tag{9}$$

τ polarisation $\mathcal{P}_\tau$ in decay $\tilde{\tau}_1 \to \tau\tilde{\chi}^0_1$ $\qquad \mathcal{P}_\tau = \mathcal{P}_\tau(\theta_{\tilde{\tau}}, \tan\beta, \tilde{\chi}^0_1 \text{ mixing})$

Selection criteria $e^+_L e^-_R \to \tilde{\tau}^+_1 \tilde{\tau}^-_1$ at $\sqrt{s} = 400$ GeV

```
nr  cut                              min       max      eff
------------------------------------------------------------
 0. n_charge, n_veto              2    6         1     0.931
 1. n_jets                             2         4     0.834
 2. n_taus                             2         4     0.829
 3. n_leptons                          0         2     0.780
 4. E_jet (GeV)                      2.5     100.0     0.739
 5. Q*cos_theta_jet               -0.950     0.750     0.597
 8. mass tau_jet (GeV)                       2.000     0.547
11. delta phi_(l,di-jet) (deg)               160.0     0.426
12. cos theta_P_miss                          0.95     0.424
13. p_T (GeV)                       10.0     200.0     0.400

 efficiency SUSY      0.3999

tau decay statistics
--------------------
            e      mu      pi     rho    3_pi     sum
e           0     510     529    1097    1125    3261
mu          0       0     470    1040    1121    2631
pi          0       0     200     783     819    1802
rho         0       0       0     821    1786    2607
3_pi        0       0       0       0     895     895
sum         0     510    1199    3741    5746   11196

 lepton energy       E_min 12.19       E_max 83.81
```

Leptonic τ decays not useful and discarded due to large WW background
Analysed decay modes & branching ratios

$$\mathcal{B}(\tau \to \pi\nu_\tau) = 0.111,\ \mathcal{B}(\tau \to \rho\nu_\tau) = 0.254,\ \mathcal{B}(\tau \to 3\pi\nu_\tau) = 0.194$$

$m_{\tilde{\tau}_1}$ from τ decays $\tau \to \rho\,\nu_\tau \to \pi^\pm\pi^0\,\nu_\tau$ and $\tau \to 3\pi\,\nu_\tau \to \pi^\pm\pi^\pm\pi^\mp\,\nu_\tau + \pi^\pm\pi^0\pi^0\,\nu_\tau$
E_ρ, $E_{3\pi}$ sensitive to $m_{\tilde{\tau}_1}$, almost independent of $\mathcal{P}_\tau$

Analysis of E_ρ and $E_{3\pi}$ spectra, shown in fig. 8, assuming $m_{\tilde{\chi}^0_1}$ known

mode	$m_{\tilde{\tau}_1}$ [GeV]
E_ρ	133.3 ± 0.75
$E_{3\pi}$	133.2 ± 0.30
mean	133.2 ± 0.30
SPS 1a input	**133.2**

$\boldsymbol{\theta_{\tilde\tau}}$ from cross section A cross section measurement of $\sigma_{\tilde\tau_1\tilde\tau_1} = 137.8 \pm 2.2_{\rm stat} \pm 1.4_{\rm sys}$ fb (incl. ISR & BS) provides a $\tilde\tau$ mixing angle of $\cos 2\,\theta_{\tilde\tau} = -0.84 \pm 0.04$, see fig. 10

$\boldsymbol{\tau}$ polarisation $\boldsymbol{\mathcal{P}_\tau}$ E_π from $\tau \to \pi\,\nu_\tau$ and $z_\pi = E_\pi/E_\rho$ from $\tau \to \rho\nu_\tau \to \pi\pi^0\nu_\tau$
E_π, z_π sensitive to $\mathcal{P}_\tau$, almost independent of $m_{\tilde\tau_1}$

τ is self-analysing system – spin correlations

$\tau^-_R \to \pi^-\nu$	$\mathcal{P}_\tau = +1$	π^- emitted in forward direction	$E_\pi \nearrow$
$\tau^-_L \to \pi^-\nu$	$\mathcal{P}_\tau = -1$	π^- emitted in backward direction	$E_\pi \searrow$
$\tau^-_R \to \rho^-_L\nu$	$\mathcal{P}_\tau = +1$	$\mathrm{d}\sigma/\mathrm{d}z_\pi \propto (2z_\pi - 1)^2$	asymmetric sharing $z_\pi \to 0\,/\,1$
$\tau^-_L \to \rho^-_T\nu$	$\mathcal{P}_\tau = -1$	$\mathrm{d}\sigma/\mathrm{d}z_\pi \propto 2z_\pi(1 - z_\pi)$	equal sharing $z_\pi \to 0.5$

Analysis of E_π and z_π spectra, shown in fig. 9, $m_{\tilde\chi^0_1}$ assumed to be known

mode	$\boldsymbol{\mathcal{P}_\tau}$
$\boldsymbol{E_\pi}$	$\mathbf{0.98 \pm 0.045}$
$\boldsymbol{z_\pi = E_\pi/E_\rho}$	$\mathbf{1.02 \pm 0.038}$
mean	$\mathbf{1.00 \pm 0.035}$
SPS 1a input	**0.981**

A polarisation measurement of $\mathcal{P}_\tau = 1.00 \pm 0.035$ is not sensitive enough to determine $\tan\beta$ in SPS 1a, where one has $\delta\mathcal{P}_\tau/\delta\tan\beta = 0.3\%$

5 Summary

Simulations of slepton production $e^+e^- \to \tilde e_R\tilde e_R,\ \tilde\mu_R\tilde\mu_R,\ \tilde\tau_1\tilde\tau_1$ in the SPS 1a mSUGRA scenario under realistic experimental conditions assuming $\sqrt{s} = 400$ GeV, $\mathcal{L} = 200$ fb^{-1} and beam polarisations $\mathcal{P}_{e^-} = +0.8$, $\mathcal{P}_{e^+} = -0.6$ are presented. The slepton and neutralino $\tilde\chi^0_1$ masses as well as the polarisation $\mathcal{P}_{\tilde\tau_1\to\tau\tilde\chi^0_1}$ and mixing parameter $\theta_{\tilde\tau}$ of the third generation can be accurately determined with moderate integrated luminosity. Improvements on $m_{\tilde e_R}$ and $m_{\tilde\mu_R}$ are possible if $\delta m_{\tilde\chi^0_1}$ can be reduced, *e.g.* by studying neutralino production and decays. An alternative method to measure selectron and smuon masses via cross section threshold scans is discussed in [11]. Other estimates on SPS 1a sparticle masses can be found in [8] and [12] (not based on detailed simulations).

$\boldsymbol{\tilde e_R}$	$\boldsymbol{m_{\tilde e_R} = 142.99 \pm 0.08}$ **GeV**	$\boldsymbol{m_{\tilde\chi^0_1} = 96.05 \pm 0.10}$ **GeV**
$\boldsymbol{\tilde\mu_R}$	$\boldsymbol{m_{\tilde\mu_R} = 143.15 \pm 0.17}$ **GeV**	$\boldsymbol{m_{\tilde\chi^0_1} = 96.10 \pm 0.21}$ **GeV**
$\boldsymbol{\tilde\tau_1}$	$\boldsymbol{m_{\tilde\tau_1} = 133.2 \pm 0.30}$ **GeV**	**—**
	$\boldsymbol{\cos 2\,\theta_{\tilde\tau} = -0.84 \pm 0.04}$	$\boldsymbol{\mathcal{P}_\tau = 1.00 \pm 0.035}$

Acknowledgement I want to thank G. Moortgat-Pick for the stimulating discussions on the stau sector and for providing the plot of fig. 10.

References

[1] TESLA Technical Design Report, DESY 2001-011, Part III: *Physics at an* e^+e^- *Linear Collider* [hep-ph/0106315], Part IV: *A Detector for TESLA*.

[2] B.C. Allanach et al., Eur. Phys. J. C 25 (2002) 113;
N. Ghodbane, H.-U. Martyn, hep-ph/0201233.

[3] PYTHIA, T. Sjöstrand et al., Comput. Phys. Commun. 135 (2001) 238.

[4] CIRCE, T. Ohl, Comput. Phys. Commun. 101 (1997) 269.

[5] TAUOLA, S. Jadach et al., Comput. Phys. Commun. 76 (1993) 361.

[6] SIMDET, M. Pohl, J. Schreiber, DESY-02-061, hep-ex/0206009.

[7] J. Feng, D. Finell, Phys. Rev. D 49 (1994) 2369.

[8] M. Dima et al., Phys. Rev. D 65 (2002) 71701.

[9] M.M. Nojiri, Phys. Rev. D 51 (1995) 6281;
M.M. Nojiri, K. Fujii, T. Tsukamoto, Phys. Rev. D 54 (1996) 6756.

[10] E. Boos et al., Eur. Phys. J. C 30 (2003) 395.

[11] A. Freitas, A. von Manteuffel, proceedings SUSY 02, DESY Hamburg, Germany, 2002, hep-ph/0211105.

[12] P. Grannis, talk at LCWS 02, Jeju Island, Korea, 2002, hep-ex/0211002.

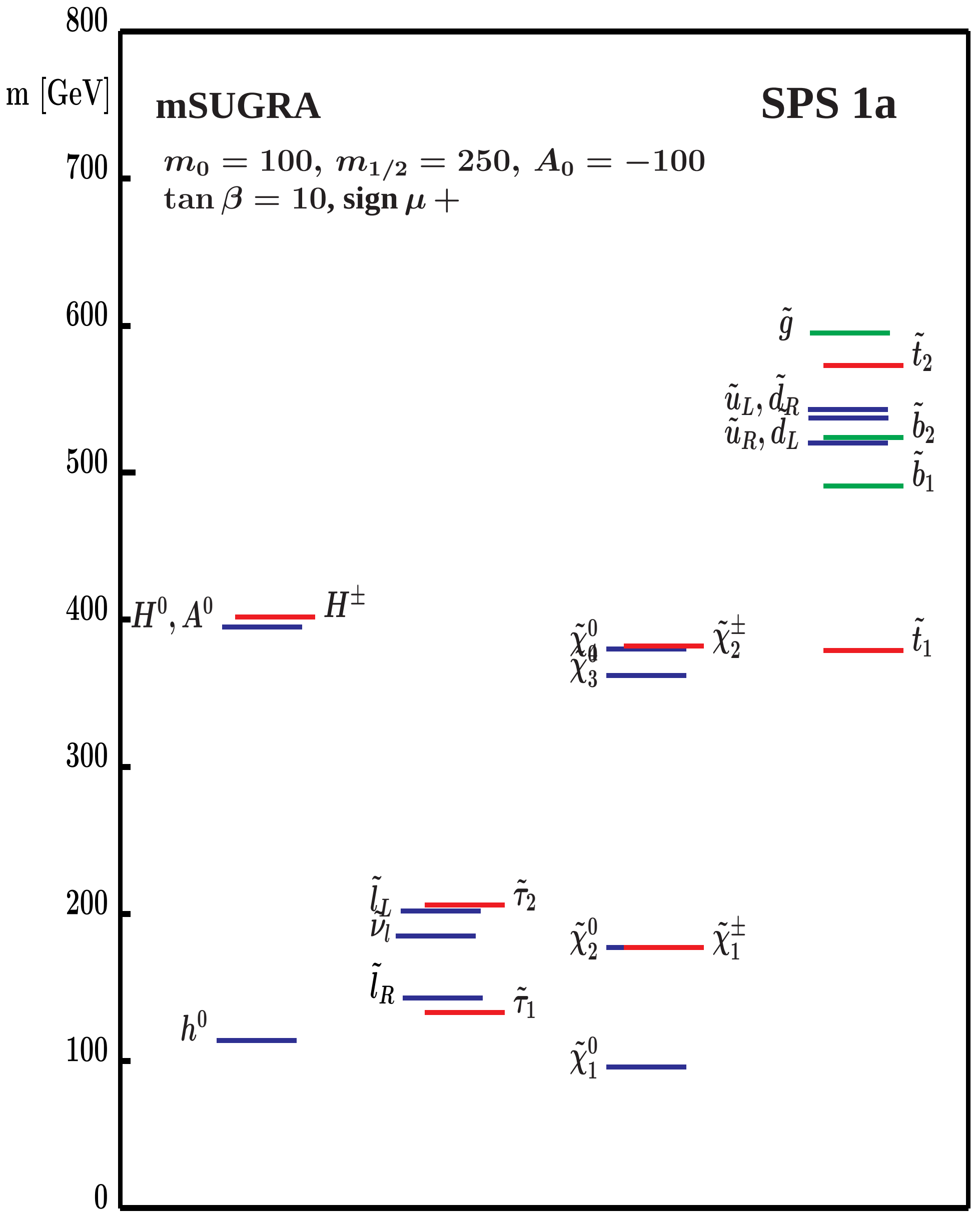

Figure 1: Particle spectrum of mSUGRA benchmark scenario SPS 1a

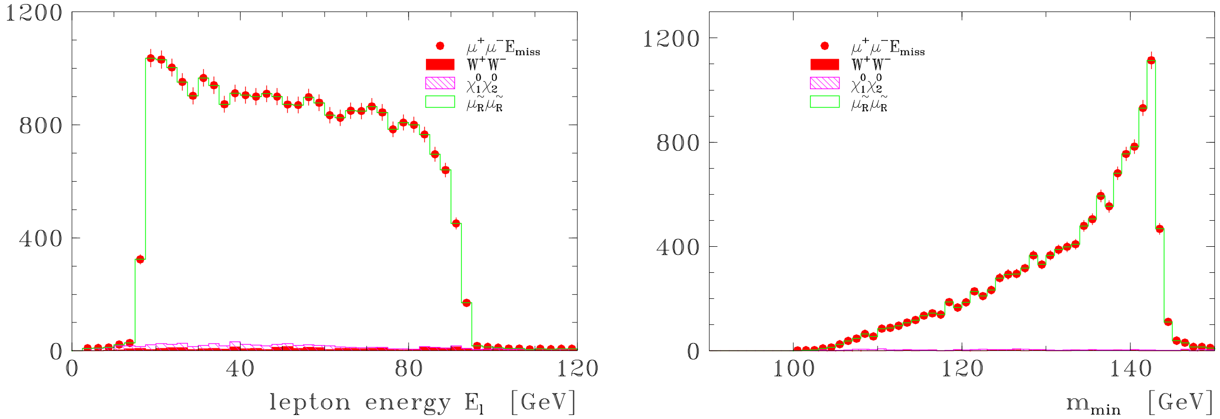

Figure 2: Energy spectrum E_μ of muons (left) and minimum mass $m_{\min}(\tilde{\mu}_R)$ (right) from the reaction $e_L^+ e_R^- \to \tilde{\mu}_R^+ \tilde{\mu}_R^- \to \mu^+ \tilde{\chi}_1^0\ \mu^- \tilde{\chi}_1^0$; mSUGRA model SPS 1a at $\sqrt{s} = 400$ GeV and $\mathcal{L} = 200\ \mathrm{fb}^{-1}$

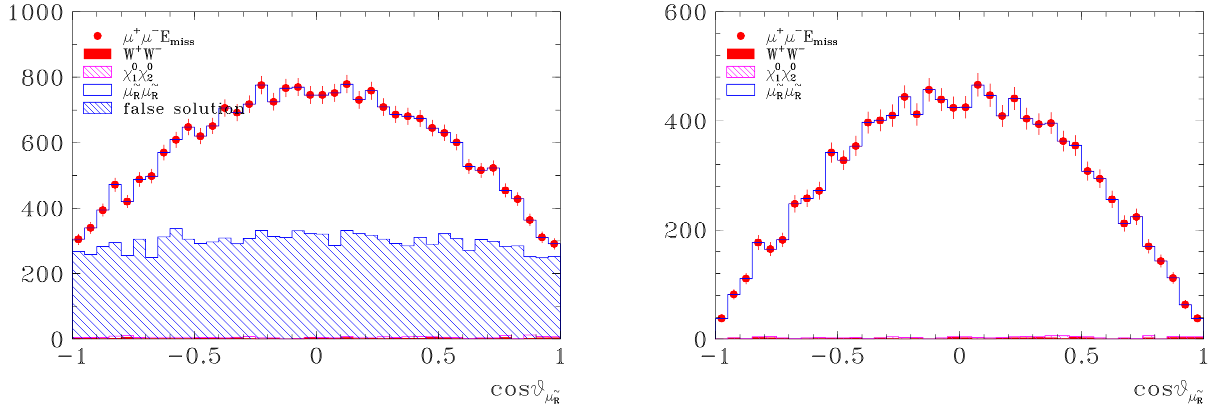

Figure 3: Polar angle distribution of $\tilde{\mu}_R$ with (left) and without (right) contribution of false solution in the reaction $e_L^+ e_R^- \to \tilde{\mu}_R^+ \tilde{\mu}_R^- \to \mu^+ \tilde{\chi}_1^0\ \mu^- \tilde{\chi}_1^0$; mSUGRA model SPS 1a at $\sqrt{s} =$ 400 GeV and $\mathcal{L} = 200\ \mathrm{fb}^{-1}$

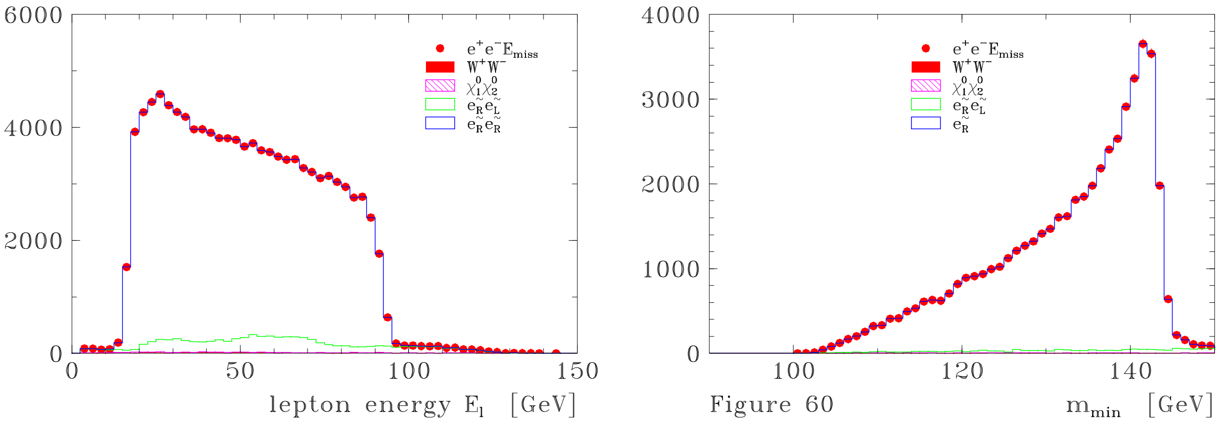

Figure 4: Energy spectrum E_e of electrons (left) and minimum mass $m_{\min}(\tilde{e}_R)$ (right) from the reaction $e^+_L e^-_R \rightarrow \tilde{e}^+_R \tilde{e}^-_R \rightarrow e^+ \tilde{\chi}^0_1 \; e^- \tilde{\chi}^0_1$; mSUGRA model SPS 1a at $\sqrt{s} = 400$ GeV and $\mathcal{L} = 200\ \text{fb}^{-1}$

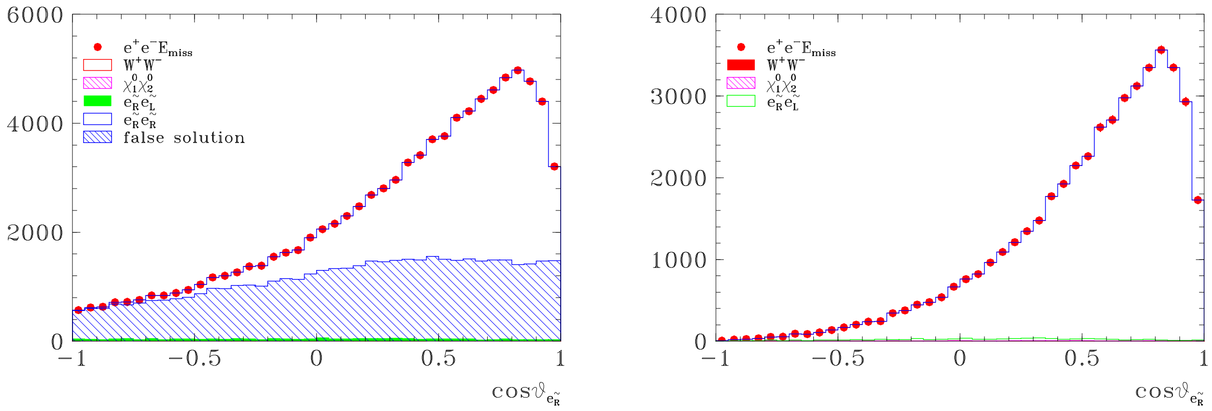

Figure 5: Polar angle distribution of $\tilde{e}_R$ with (left) and without (right) contribution of false solution in the reaction $e^+_L e^-_R \rightarrow \tilde{e}^+_R \tilde{e}^-_R \rightarrow e^+ \tilde{\chi}^0_1 \; e^- \tilde{\chi}^0_1$; mSUGRA model SPS 1a at $\sqrt{s} = 400$ GeV and $\mathcal{L} = 200\ \text{fb}^{-1}$

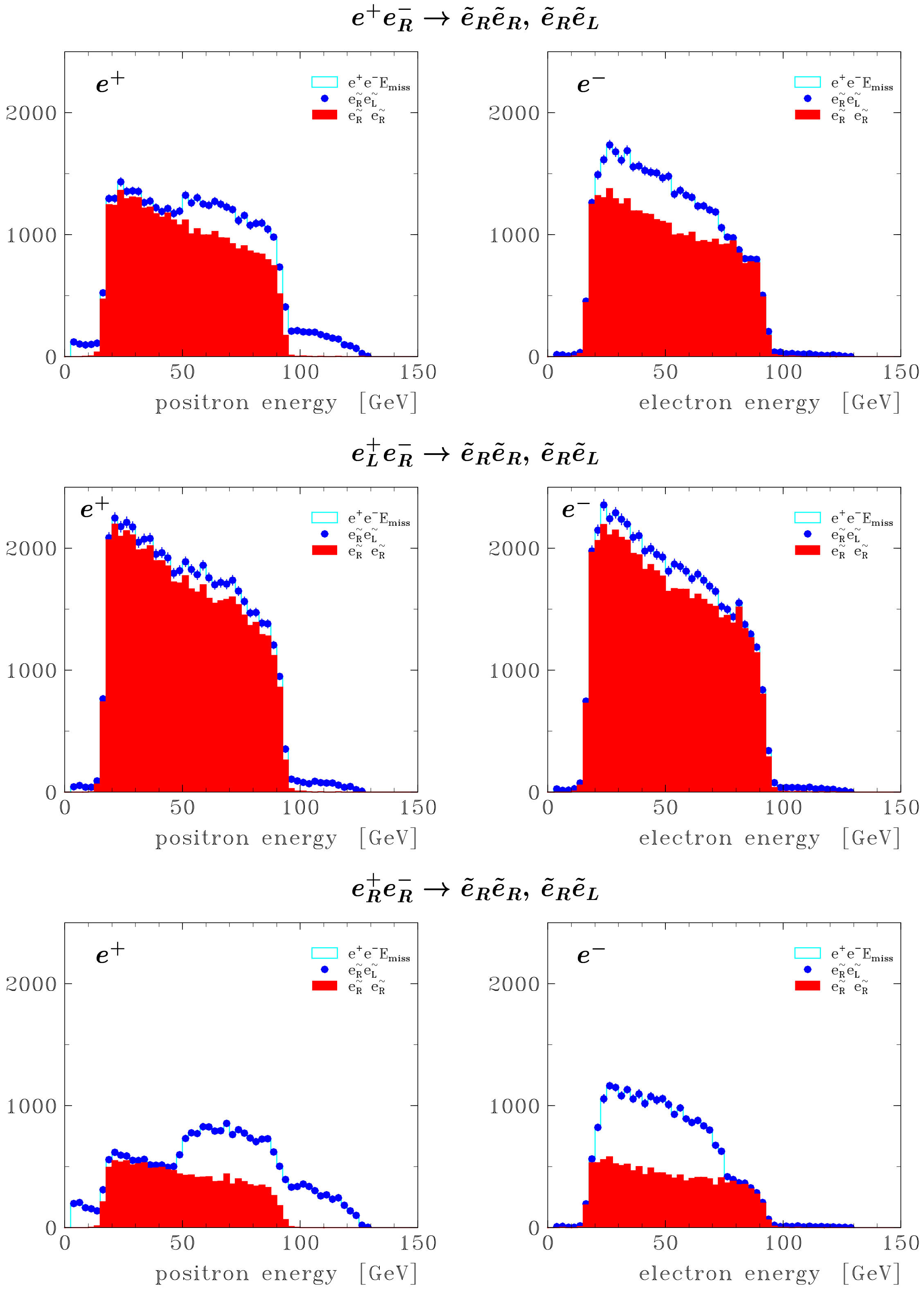

$e^+e^-_R \to \tilde{e}_R\tilde{e}_R,\ \tilde{e}_R\tilde{e}_L$

$e^+_L e^-_R \to \tilde{e}_R\tilde{e}_R,\ \tilde{e}_R\tilde{e}_L$

$e^+_R e^-_R \to \tilde{e}_R\tilde{e}_R,\ \tilde{e}_R\tilde{e}_L$

Figure 6: $e^{\pm}$ energy spectra from $e^+e^- \to \tilde{e}_R\tilde{e}_R + \tilde{e}_R\tilde{e}_L$ production with polarisations $\mathcal{P}_{e^-} = +0.8$, $\mathcal{P}_{e^+}$ variable for SPS 1a scenario assuming $\sqrt{s} = 400\,\text{GeV}$ and $\mathcal{L} = 200\,\text{fb}^{-1}$

$\boldsymbol{e^+ e^-_L \to \tilde{e}_R \tilde{e}_R,\ \tilde{e}_R \tilde{e}_L}$

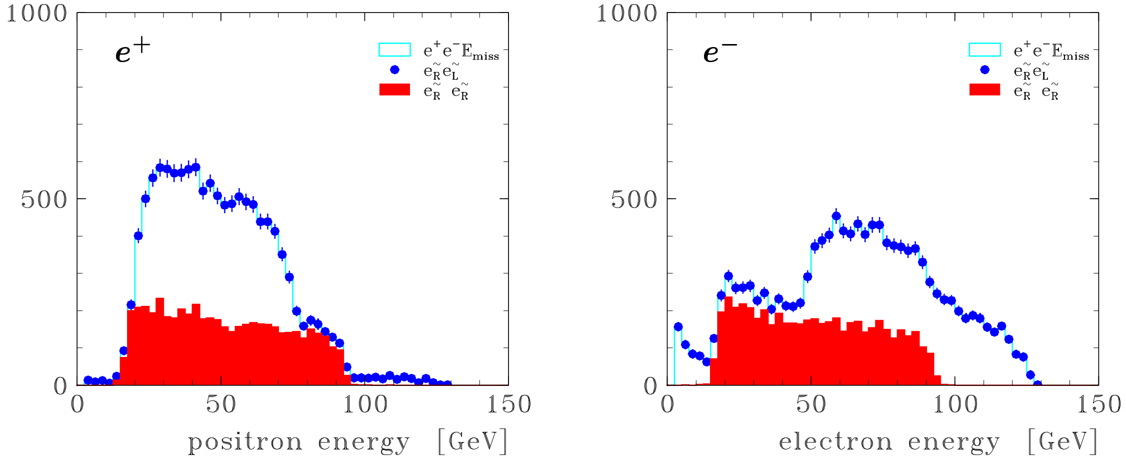

$\boldsymbol{e^+_R e^-_L \to \tilde{e}_R \tilde{e}_R,\ \tilde{e}_R \tilde{e}_L}$

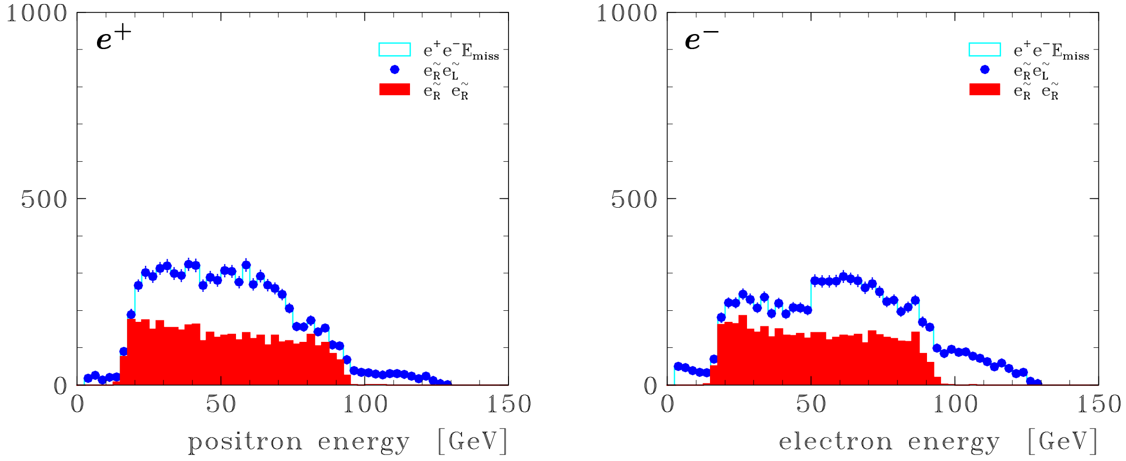

$\boldsymbol{e^+_L e^-_L \to \tilde{e}_R \tilde{e}_R,\ \tilde{e}_R \tilde{e}_L}$

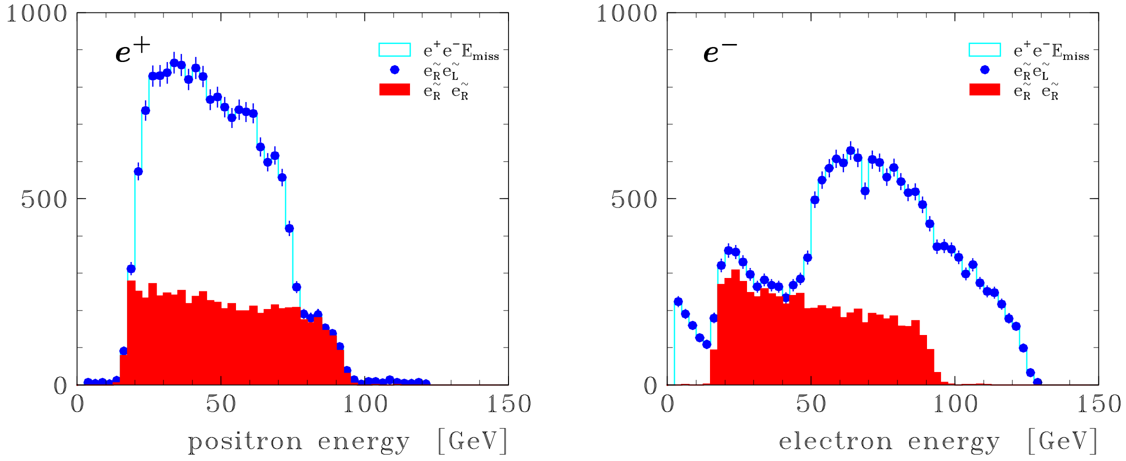

Figure 7: $e^\pm$ energy spectra from $e^+e^- \to \tilde{e}_R\tilde{e}_R + \tilde{e}_R\tilde{e}_L$ production with polarisations $\mathcal{P}_{e^-} = -0.8$, $\mathcal{P}_{e^+}$ variable for SPS 1a scenario assuming $\sqrt{s} = 400\,\text{GeV}$ and $\mathcal{L} = 200\,\text{fb}^{-1}$

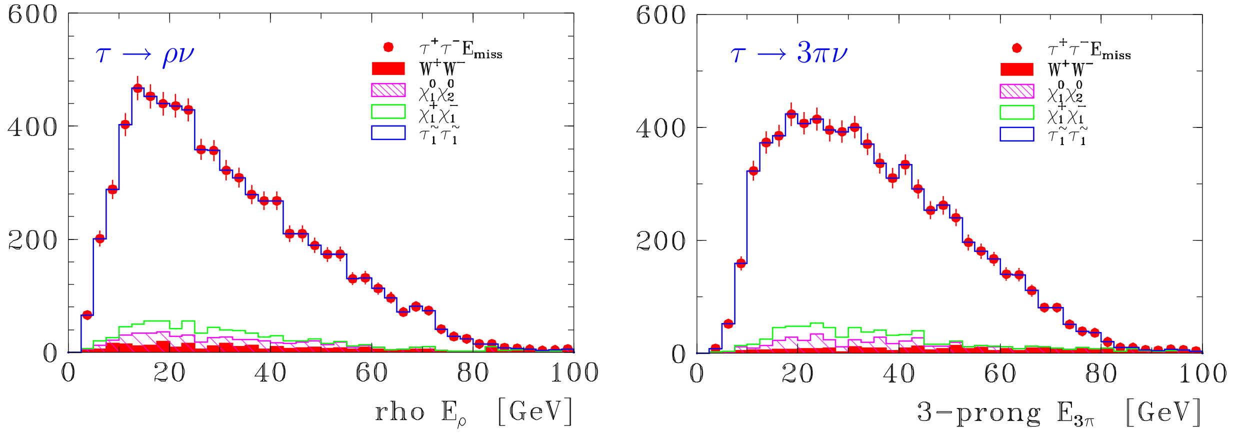

Figure 8: Hadron energy spectra E_ρ of $\tau \longrightarrow \rho\nu_\tau$ and $E_{3\pi}$ of $\tau \longrightarrow 3\pi\nu_\tau$ decays from the reaction $e^+_L e^-_R \longrightarrow \tilde{\tau}_1^+\tilde{\tau}_1^1 \longrightarrow \tau^+\tilde{\chi}_1^0\ \tau^-\tilde{\chi}_1^0$ in SPS 1a scenario assuming $\sqrt{s} = 400\,\mathrm{GeV}$ and $\mathcal{L} = 200\,\mathrm{fb}^{-1}$

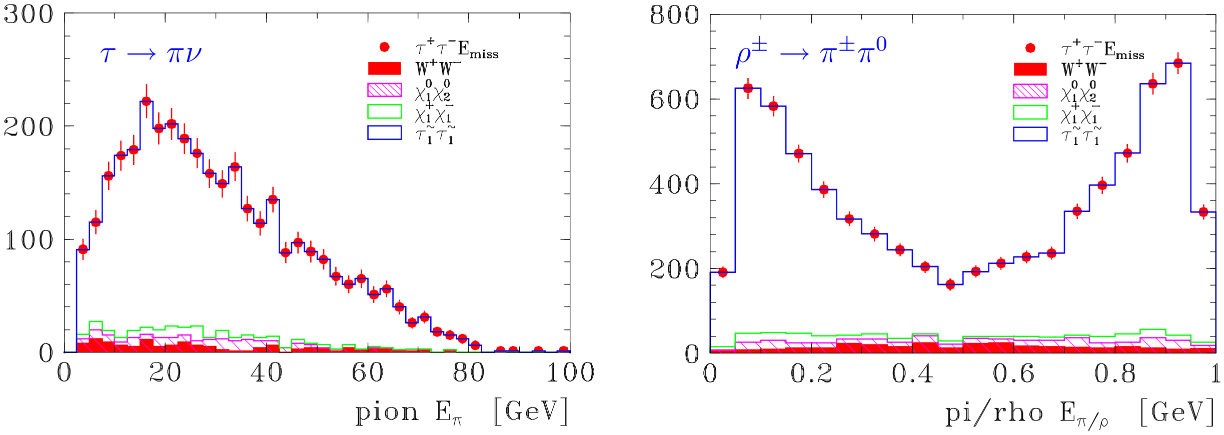

Figure 9: Pion energy spectrum E_π of $\tau \longrightarrow \pi\nu_\tau$ and ratio $z_\pi = E_\pi/E_\rho$ of $\tau \longrightarrow \rho\nu_\tau$ decays from the reaction $e^+_L e^-_R \longrightarrow \tilde{\tau}_1^+\tilde{\tau}_1^1 \longrightarrow \tau^+\tilde{\chi}_1^0\ \tau^-\tilde{\chi}_1^0$ in SPS 1a scenario assuming $\sqrt{s} = 400\,\mathrm{GeV}$ and $\mathcal{L} = 200\,\mathrm{fb}^{-1}$

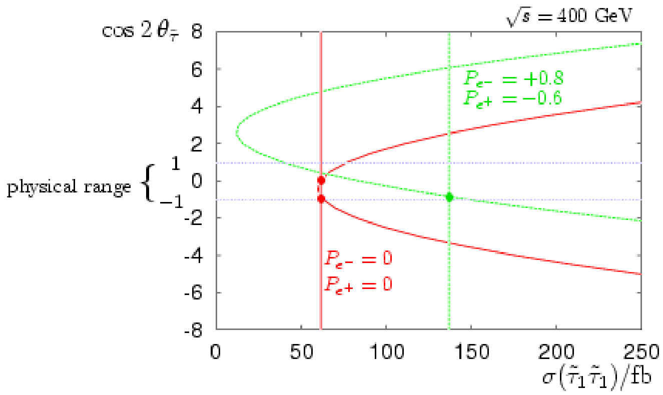

Figure 10: Mixing angle angle $\cos 2\theta_{\tilde{\tau}}$ versus cross section $\sigma_{\tilde{\tau}_1\tilde{\tau}_1}$ at $\sqrt{s} = 400$ GeV for mSUGRA scenario SPS 1a